Implications of PREX-2 data on the electron-neutrino opacity in dense matter

Parada T. P. Hutauruk *

Department of Physics, Pukyong National University (PKNU), Busan 48513, Korea

(Received 9 June 2021; accepted 24 November 2021; published 10 December 2021)

Motivated by the recent measurement of the neutron distribution radius of ^{208}Pb from the PREX-2 data, I study the effects of the new G3(M) parameter set constrained by PREX-2 data on the electron-neutrino scattering in dense matter using the extended relativistic mean-field (E-RMF) model. I employ the G3(M) parameter set to describe the nuclear matter. The obtained equation of state for the G3(M) parameter set has an excellent agreement with experimental data and the chiral effective field theory calculation with N^{3}LO 3N forces. I analyze both the differential cross section of the electron-neutrino and electron-neutrino mean free path to observe their sensitivity to the G3(M) parameter set. One finds that the differential cross sections of electron-neutrinos for different baryon densities have higher values compared with those obtained for the TM1e and FSU Garnet parameter sets. The higher cross section decreases the electron-neutrino mean free path.

DOI: 10.1103/PhysRevC.104.065802

I. INTRODUCTION

Neutrinos play a very important role in the evolution processes of the neutron star (NS) and the supernova, which corresponds with the cooling rate of the neutron star, which is controlled by neutrinos emmision [1,2]. The neutrinos emission and scattering are sensitive to the equation of state (EOS) of nuclear matter [3–7] and the nucleon effective mass M_N^* [7].

Recently, a measurement of parity-violating asymmetry $A_{\rm PV}$ at transferred momentum $\mathbf{q} = 0.3978/\text{fm}$ in ^{208}Pb by the Lead Radius Experiment (PREX-2) reported an accurate determination of the neutron skin thickness of ^{208}Pb with a precision approximately equal to 1% [8]. Combining analysis of PREX-2 [8] with the previous measurement of PREX [9] gives

$$\Delta R_{\rm skin} = R_n - R_p = (0.283 \pm 0.071)\ \text{fm}, \qquad (1)$$

where R_n and R_p are respectively the root-mean-squared radii for the neutron and proton density distributions. The accurate measurement of neutron skin thickness ($\Delta R_{np} = R_n - R_p$) is a very important and useful quantity to constrain the EOS for finite nuclei and nuclear matter. The reliable EOS can be obtained by refitting the appropriate parameters within the theoretical models to reproduce the properties of finite nuclei. The better constraint on the EOS, in particular, at high baryon density will lead us to gain a deeper understanding of the properties of neutron stars, such as the size, mass, and particle composition of β-stable matter. Interestingly, it may also affect the electron-neutrino scattering with matter inside the NS. Henceforth electron-neutrino is simply referred as "neutrino".

In recent works, several attempts have been made to investigate the implications of PREX-2 data on the EOS [10], symmetry energy [11], and electric dipole polarizability [12]. In addition, the implications of new EOS constrained by PREX-2 data on the properties of neutron stars have been studied [10,11]. A very recent work of Ref. [10] has developed a new parameter set of the E-RMF model through fine-tuning parameters (Λ_ω, which relates to $\eta_{2\rho}$ in the E-RMF model of the present work, and g_ρ parameters) to fit the R_n of PREX-2 data [8]. The new parameter set is labeled as the G3(M) parameter set. Thus, it was used to validate the constraint from the GW170817 binary NS merger to understand the properties of neutron stars. The G3(M) parameter set relatively gives a better prediction for finite and nuclear matter. Further detailed explanations of this G3(M) parameter set can be found in Ref. [10]. So far, in the literature, this G3(M) parameter set has not yet been applied to the neutrino scattering with dense matter. Therefore, it will be very interesting and challenging to investigate how sensitive the EOS and neutrino scattering observable are to the new G3(M) parameter set constrained by an accurate measurement of the PREX-2 data [8].

In present work, I perform the extended relativistic mean-field model with the modified G3(M) parameter set [10] constrained by the PREX-2 data [8]. The E-RMF model has been widely used to study the finite nuclei and infinite nuclear matter [13–15]. The predictions of this model are relatively good for describing the bulk properties of finite nuclei at saturation density and the properties of neutron stars. In this work, I calculate the EOS, particle fractions of the constituents of β-stable matter, which consist of electrons, neutrons, protons, and muons, differential cross section (DCRS) of the neutrino, and neutrino mean free path (NMFP). I then observe the sensitivity of these quantities to the G3(M) parameter set.

One finds that the binding energy per nucleon E_B/A for pure neutron matter (PNM) with the G3(M) parameter set is softer than those obtained for the TM1e [16] and FSU Garnet [17] parameter sets at low baryon density. However, the E_B/A for the G3(M) parameter set is rather stiffer than that obtained

*phutauruk@gmail.com

for the FSU Garnet parameter set and is the same as that obtained for the TM1e parameter set. The PNM pressure for the G3(M) parameter set fits well with the asy-soft of the flow data [18] at intermediate ρ_B/ρ_0, with ρ_B and ρ_0 being respectively the baryon and saturation densities. It is in good agreement with the asy-stiff of the flow data [18] at higher ρ_B/ρ_0. The sound velocities $v_s(c)$ for the G3(M), TM1e, and FSU Garnet parameter sets predict the same sound velocity at around saturation density ($\rho_B/\rho_0 \simeq 1$) and at $\rho_B/\rho_0 \simeq 3.7$.

Total differential cross sections of neutrinos for the GM(3) parameter set are found to be higher than those obtained for the TM1e and FSU Garnet parameter sets for different baryon densities. As consequences, the NMFP for the G3(M) parameter set is lower than the NMFPs obtained for the TM1e and FSU Garnet parameter sets. The higher DCRS or lower NMFP for the G3(M) parameter set is expected because the nucleon effective mass M_N^* is higher than those obtained for the FSU Garnet and TM1e parameter sets.

This paper is organized as follows. In Sec. II, I briefly introduce the effective Lagrangian for nuclear matter within the E-RMF model with the G3(M) parameter set. I then calculate the EOS such as the binding energy, pressure, and sound velocity for pure neutron matter. In Sec. III, I present the expression for both the differential cross section of the neutrino and neutrino mean free path, and I then observe their sensitivity to the G3(M) parameter set as well as to the nucleon effective mass. In Sec. IV the results are presented and their implications are discussed. Section V is devoted to a summary.

II. E-RMF MODEL

Here I briefly introduce the EOS of dense matter that is used to describe the constituents of matter. I employ the E-RMF model with the modified G3(M) parameter set, as mentioned above already. The effective Lagrangian for the E-RMF model is given by [15,19]

$$\mathscr{L}_{\rm ERMF} = \mathscr{L}_{\rm NM} + \mathscr{L}_\sigma + \mathscr{L}_\omega + \mathscr{L}_\rho + \mathscr{L}_\delta + \mathscr{L}_{\sigma\omega\rho}, \quad (2)$$

where the interaction Lagrangian of the nucleons and mesons is defined by

$$\mathscr{L}_{\rm NM} = \sum_{j=n,p} \bar{\psi}_j \Big[i\gamma^\mu \partial_\mu - (M_N - g_\sigma \sigma - g_\delta \boldsymbol{\tau}_j \cdot \boldsymbol{\delta}) - \Big(g_\omega \gamma^\mu \omega_\mu + \frac{1}{2} g_\rho \gamma^\mu \boldsymbol{\tau}_j \cdot \boldsymbol{\rho}_\mu \Big) \Big] \psi_j, \quad (3)$$

where the sum stands for the neutrons and protons, M_N is the nucleon mass, and $\boldsymbol{\tau}_j$ are the isospin matrices. The g_σ, g_ω, g_ρ, and g_δ are respectively the coupling constants for the σ, ω, ρ, and δ mesons. The self-interaction Lagrangians for the σ, ω, ρ, and δ mesons are expressed by

$$\mathscr{L}_\sigma = \frac{1}{2}\big(\partial_\mu \sigma \partial^\mu \sigma - m_\sigma^2 \sigma^2\big) - \frac{\kappa_3}{6M_N} g_\sigma m_\sigma^2 \sigma^3 - \frac{\kappa_4}{24 M_N^2} g_\sigma^2 m_\sigma^2 \sigma^4, \quad (4)$$

$$\mathscr{L}_\omega = -\frac{1}{4}\omega_{\mu\nu}\omega^{\mu\nu} + \frac{1}{2} m_\omega^2 \omega_\mu \omega^\mu + \frac{1}{24}\xi_0 g_\omega^2 (\omega_\mu \omega^\mu)^2, \quad (5)$$

TABLE I. The complete parameter sets for the G3(M) that determined by readjusting to the PREX-2 data [8], TM1e [16], and FSU Garnet [17]. The nucleon mass M_N is 939 MeV and all coupling constants are dimensionless. The unit of k_3 is in fm^{-1}.

Parameters	G3(M)	TM1e	FSU Garnet
m_s/M_N	0.559	0.511	0.529
m_ω/M_N	0.832	0.783	0.833
m_ρ/M_N	0.820	0.770	0.812
m_δ/M_N	1.043	0.980	0.000
$g_s/4\pi$	0.782	0.798	0.837
$g_\omega/4\pi$	0.923	1.004	1.091
$g_\rho/4\pi$	0.872	1.112	1.105
$g_\delta/4\pi$	0.160	0.000	0.000
k_3	2.606	−1.021	1.368
k_4	1.694	0.124	−1.397
β_ω	−0.484	0.000	0.000
ξ_0	1.010	2.689	4.410
η_1	0.424	0.000	0.000
η_2	0.114	0.000	0.000
η_ρ	0.645	0.000	0.000
$\eta_{1\rho}$	0.000	0.000	0.000
$\eta_{2\rho}$	18.257	50.140	50.698
α_1	2.000	0.000	0.000
α_2	−1.468	0.000	0.000
$f_\omega/4$	0.220	0.000	0.000
$f_\rho/4$	1.239	0.000	0.000
β_σ	−0.087	0.000	0.000

$$\mathscr{L}_\rho = -\frac{1}{4}\boldsymbol{\rho}_{\mu\nu} \cdot \boldsymbol{\rho}^{\mu\nu} + \frac{1}{2} m_\rho^2 \boldsymbol{\rho}_\mu \cdot \boldsymbol{\rho}^\mu, \quad (6)$$

$$\mathscr{L}_\delta = \frac{1}{2}\partial_\mu \boldsymbol{\delta} \cdot \partial^\mu \boldsymbol{\delta} - \frac{1}{2} m_\delta^2 \boldsymbol{\delta}^2. \quad (7)$$

Here m_σ, m_ω, m_ρ, and m_δ are the meson masses, and $\omega^{\mu\nu}$ and $\rho^{\mu\nu}$ are the field tensors for the ω and ρ mesons, which are respectively defined as $\omega^{\mu\nu} = \partial^\mu \omega^\nu - \partial^\nu \omega^\mu$ and $\boldsymbol{\rho}^{\mu\nu} = \partial^\mu \boldsymbol{\rho}^\nu - \partial^\nu \boldsymbol{\rho}^\mu - g_\rho(\boldsymbol{\rho}^\mu \times \boldsymbol{\rho}^\nu)$.

The nonlinear cross interaction Lagrangian of σ, ω, and ρ mesons is given by

$$\mathscr{L}_{\sigma\omega\rho} = \frac{\eta_1}{2M_N} g_\sigma m_\omega^2 \sigma \omega_\mu \omega^\mu + \frac{\eta_2}{4M_N^2} g_\sigma^2 m_\omega^2 \sigma^2 \omega_\mu \omega^\mu + \frac{\eta_\rho}{2M_N} g_\sigma m_\rho^2 \sigma \boldsymbol{\rho}_\mu \cdot \boldsymbol{\rho}^\mu + \frac{\eta_{1\rho}}{4M_N^2} g_\sigma^2 m_\rho^2 \sigma^2 \boldsymbol{\rho}_\mu \cdot \boldsymbol{\rho}^\mu + \frac{\eta_{2\rho}}{4M_N^2} g_\omega^2 m_\rho^2 \omega_\mu \omega^\mu \boldsymbol{\rho}_\mu \cdot \boldsymbol{\rho}^\mu, \quad (8)$$

where κ_3, κ_4, ξ_0, η_1, η_2, η_ρ, $\eta_{1\rho}$, and $\eta_{2\rho}$ are the coupling constants. The complete values of the coupling constants in the Lagrangian in Eqs. (3)–(8) are summarized in Table I.

The Lagrangian density for the electron and muon is given by

$$\mathscr{L}_l = \sum_{l=e,\mu} \bar{\psi}_l (i\gamma_\mu \partial^\mu - m_l)\psi_l, \quad (9)$$

with m_l being the lepton mass. Once the Lagrangian is given, the particle composition of the dense matter with n, p, e, and μ can be obtained through the constraint of β-stability that

states the relation of the chemical potential as

$$\mu_n - \mu_p = \mu_e, \quad \mu_e = \mu_\mu, \tag{10}$$

and the charge neutrality as

$$\rho_p = \rho_e + \rho_\mu, \tag{11}$$

where the leptons are treated as relativistic ideal Fermi gases. The terms $\mu_{p,n} = \frac{\partial \mathscr{E}}{\rho_{p,n}}$ are the chemical potentials of protons and neutrons, respectively, and ρ_p, ρ_e, and ρ_μ are the proton, electron, and muon densities, respectively. The chemical potentials for leptons are given by $\mu_{l=e,\mu} = \sqrt{k^2_{F_{l=e,\mu}} + m^2_{l=e,\mu}}$. The total baryon density is defined by $\rho_B = \rho_p + \rho_n$, with ρ_n being the neutron density.

The difference between the G3(M) parameter set and both TM1e and FSU Garnet parameter sets is the G3(M) parameter set has nonzero coupling constants η_1, η_2, η_ρ, α_1, α_2, f_ω, f_ρ, β_σ, and β_ω, whereas for the TM1e and FSU Garnet parameter sets, those coupling constants are set equal to zero as shown in Table I.

Besides the difference in those coupling constants, the difference is also given by the value of the g_δ coupling constant, which contributes to stiffening the EOS at high density as well as the symmetry energy at subsaturation density. For the FSU Garnet and TM1e parameter sets, they have different values for m_δ.

The nonlinear cross-coupling constants play an important role in obtaining a better EOS for PNM that affects the particle fractions, neutrino cross section, mean free path. Here I emphasize again that in the G3(M) parameter set, the nonlinear cross-coupling constant of the ρ meson with the ω meson, $\eta_{2\rho}$, and the coupling constant of the ρ meson, g_ρ, are obtained by fine-tuning these parameters to fit the neutron-skin thickness of ^{208}Pb from the PREX-2 data, making a crucial different between the G3(M) parameter set and the TM1e and FSU Garnet parameter sets.

Using the effective Lagrangian in Eq. (2), the energy density $\mathscr{E}$ and pressure P of the dense matter can be determined using the standard procedure by solving the energy-momentum tensor

$$T_{\mu\nu} = \sum_k \partial_\nu \phi_k \frac{\partial \mathscr{L}}{\partial(\partial^\mu \phi_k)} - g_{\mu\nu}\mathscr{L}, \tag{12}$$

where ϕ_k are all the fields in the Lagrangian in Eq. (2). Thus, the energy density is obtained by taking the zeroth component of the energy-momentum tensor $\langle T_{00}\rangle$ that gives $\mathscr{E} = \langle T_{00}\rangle$, and the pressure is obtained from the energy-momentum tensor third component $\langle T_{kk}\rangle$ that gives $P = \sum_k \frac{1}{3}\langle T_{kk}\rangle$. The energy density and pressure expressions for PNM are respectively given by

$$\begin{aligned}\mathscr{E} = {} & \sum_{i=n,p} \frac{2}{(2\pi)^3}\int_0^{k_F^i} d^3k \sqrt{\boldsymbol{k}_i^2 + M_i^{*2}} + \rho_B g_\omega \omega - \frac{1}{24}\xi_0 g_\omega^2 \omega^4 \\ & + \frac{1}{2}m_\sigma^2\sigma^2\left(1 + \frac{\kappa_3}{3M_N}g_\sigma\sigma + \frac{\kappa_4}{12M_N^2}g_\sigma^2\sigma^2\right) \\ & - \frac{1}{2}m_\omega^2\omega^2\left(1 + \frac{\eta_1}{M_N}g_\sigma\sigma + \frac{\eta_2}{2M_N^2}g_\sigma^2\sigma^2\right) \\ & - \frac{1}{2}m_\rho^2\rho^2\left(1 + \frac{\eta_\rho}{M_N}g_\sigma\sigma + \frac{\eta_{1\rho}}{2M_N^2}g_\sigma^2\sigma^2\right) \\ & - \frac{\eta_{2\rho}}{2}g_\rho^2 g_\omega^2 \rho^2\omega^2 + \frac{1}{2}\rho_3 g_\rho \rho + \frac{1}{2}m_\delta^2\delta^2 \end{aligned} \tag{13}$$

and

$$\begin{aligned} P = {} & \sum_{i=n,p} \frac{1}{3}\frac{2}{(2\pi)^3}\int_0^{k_F^i} d^3k \frac{\boldsymbol{k}_i^2}{\sqrt{\boldsymbol{k}_i^2 + M_i^2}} + \frac{1}{24}\xi_0 g_\omega^2 \omega^4 \\ & - \frac{1}{2}m_\sigma^2\sigma^2\left(1 + \frac{\kappa_3}{3M_N}g_\sigma\sigma + \frac{\kappa_4}{12M_N^2}g_\sigma^2\sigma^2\right) \\ & + \frac{1}{2}m_\omega^2\omega^2\left(1 + \frac{\eta_1}{M_N}g_\sigma\sigma + \frac{\eta_2}{2M_N^2}g_\sigma^2\sigma^2\right) \\ & + \frac{1}{2}m_\rho^2\rho^2\left(1 + \frac{\eta_\rho}{M_N}g_\sigma\sigma + \frac{\eta_{1\rho}}{2M_N^2}g_\sigma^2\sigma^2\right) + \frac{\eta_{2\rho}}{2}g_\rho^2 g_\omega^2 \rho^2\omega^2 \\ & - \frac{1}{2}m_\delta^2\delta^2, \end{aligned} \tag{14}$$

where the Fermi momentum k_F is defined by $\rho_B = \frac{k_F^3}{3\pi^2}$, and $\rho_3 = \rho_p - \rho_n$.

Using the energy density in Eq. (13) and the pressure in Eq. (14), one can construct the relationship between P and $\mathscr{E}$. Thus, the sound velocity $v_s(c)$ can be straightforwardly determined from the derivative of P with respect to the energy density $\mathscr{E}$; it then gives

$$\frac{v_s}{c} = \left(\frac{\partial P}{\partial \mathscr{E}}\right)^{\frac{1}{2}}, \tag{15}$$

where c is the speed of light.

Results for the binding energy per nucleon E_B/A calculated in the E-RMF model for the G3(M), TM1e, and FSU Garnet parameter sets are shown in Fig. 1. Figure 1 shows that the

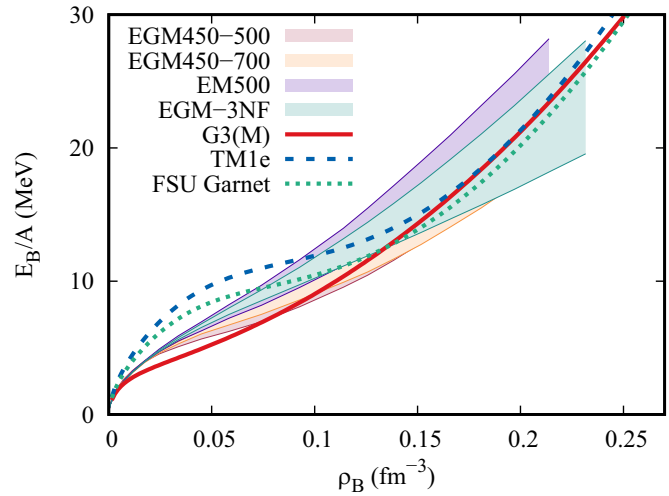

FIG. 1. Binding energy for pure neutron matter as a function of ρ_B calculated in the E-RMF model for the G3(M) [10] (solid line), TM1e [16] (dashed line), and FSU Garnet [17] (dotted line) parameter sets. The chiral effective field theory calculation with N^{3}LO 3N forces is taken from Ref. [20] (green shaded area).

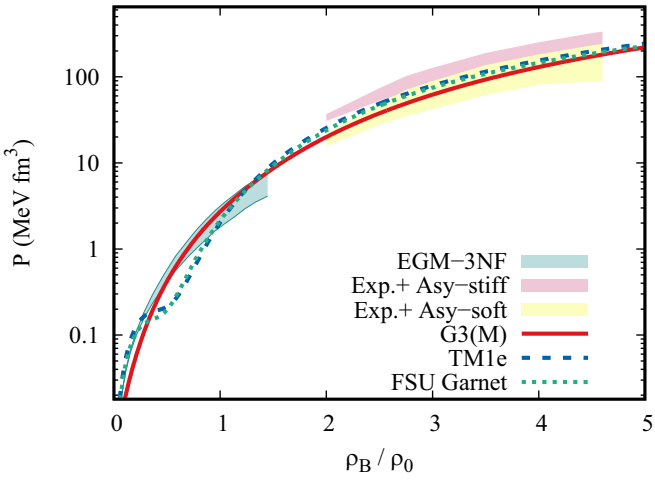

FIG. 2. Pressure for pure neutron matter as a function of ρ_B/ρ_0 calculated in the E-RMF model using the same parameter sets as used in Fig. 1. The line representations are the same as those in Fig. 1. The chiral effective field theory calculation with N^{3}LO 3N forces is taken from Ref. [20] (green shaded area). The yellow and pink shaded areas are experimental data, which are taken from Ref. [18].

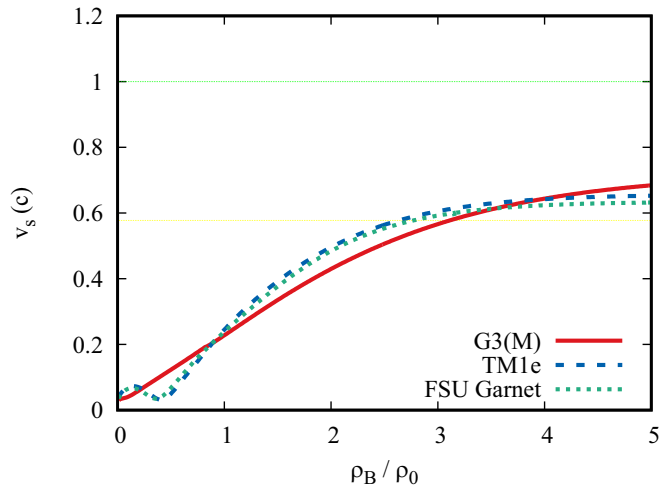

FIG. 3. Sound velocity v_s (c) (in units of the speed of light) as a function of ρ_B/ρ_0 calculated in the E-RMF model using the same parameter sets as those used in Fig. 1. The lower and upper bounds for the velocity of sound in dense matter are respectively represented by $v_s(c) = 1/\sqrt{3}$ (yellow line) and $v_s(c) = 1$ (green line).

binding energy for the G3(M) parameter set is softer at low baryon density compared with the binding energies obtained for the TM1e and FSU Garnet parameter sets. However, at intermediate and high baryon densities, the binding energy for the G3(M) parameter set is rather stiffer than that obtained for the FSU Garnet parameter set and is the same as that obtained for the TM1e parameter set. In addition, the binding energy per nucleon E_B/A for the G3(M) parameter set is in excellent agreement with the chiral effective field theory calculation with N^{3}LO 3N forces [20], in particular, at higher densities.

Figure 2 shows the pressure for PNM with the G3(M), TM1e, and FSU Garnet parameter sets compared with the experimental data [18]. The pressure for the G3(M) parameter set fits well with the asy-soft experimental data [18] at intermediate ρ_B/ρ_0. However, it overlaps with the asy-stiff experimental data [18] at higher ρ_B/ρ_0. At lower density ($\rho_B/\rho_0 \lesssim 2$), the pressure for PNM with the G3(M) parameter set has an excellent agreement with the chiral effective field theory calculation with N^{3}LO 3N forces [20].

The sound velocity calculated in the E-RMF model using the G3(M) parameter set is shown in Fig. 3. Compared with the sound velocity for the TM1e and FSU Garnet parameter sets, the G3(M) parameter set has lower sound velocity at intermediate ρ_B/ρ_0, but higher sound velocity at very lower and higher ρ_B/ρ_0. All models predict the same sound velocity at around the saturation density ($\rho_B/\rho_0 \simeq 1$) and at $\rho_B/\rho_0 \simeq 3.7$, which is a crossing point of the models. Also, all models satisfy the upper bound $v_s(c)$ constraint, meaning the models do not violate the causality.

III. NEUTRINO SCATTERING IN DENSE MATTER

A. Differential cross section

Based on the weak interaction in the standard model, the Lagrangian density for the neutrino interaction with each constituent of matter is given by the current-current interaction and it has the form [21,22]

$$\mathscr{L}^j_{\rm int} = \tilde{G}_F[\bar{\nu}\gamma^\mu(1-\gamma_5)\nu]\big(\bar{\psi}\Gamma^i_\mu\psi\big), \tag{16}$$

where $\tilde{G}_F = \frac{G_F}{\sqrt{2}}$, where $G_F = 1.023\times10^{-5}/M_N^2$ and M_N is the nucleon mass. The nucleon vertex is given by $\Gamma^j_\mu = \gamma_\mu(C^j_V - C^j_A\gamma_5)$ where $j = (n, p, e^-, \mu^-)$ stands for the constituents of matter. For the neutron, $C_V = -0.5$ and $C_A = -g_A/2$, and for the proton, $C_V = 0.5 - 2\sin^2\theta_w$ and $C_A = g_A/2$, where $g_A = 1.260$ is the axial coupling constant and $\sin^2\theta_w = 0.223$. For the electron, $C_V = 0.5 + 2\sin^2\theta_w$ and $C_A = 0.5$, whereas for the muon, $C_V = -0.5 + 2\sin^2\theta_w$ and $C_A = -0.5$. Further details of the values of C_V and C_A can be found in Refs. [6,21–23].

For the charged-current absorption reactions, the interaction Lagrangian for the lepton and baryon in Eq. (16) can be rewritten as

$$\mathscr{L}^{(\rm cc)}_{\rm int} = \tilde{G}_F C[\bar{\psi}_l\gamma^\mu(1-\gamma_5)\nu]\big(\bar{\psi}\Gamma^{(\rm cc)}_\mu\psi\big), \tag{17}$$

where $\Gamma^{(\rm cc)}_\mu = \gamma_\mu(g_V - g_A\gamma_5)$ and $\bar{\psi}_l$ are leptons. The C is the Cabibbo factor with $C = \cos\theta_c$ for strangeness $\Delta S = 0$ and $C = \sin\theta_c$ for $\Delta S = 1$. The values for g_V and g_A for the corresponding reactions can be found in Refs. [6,21–23]. Note that the DCRS for the neutral-current scattering has a similar expression as that for the charged-current absorption. The difference comes only from the values of the axial and vector coupling constants.

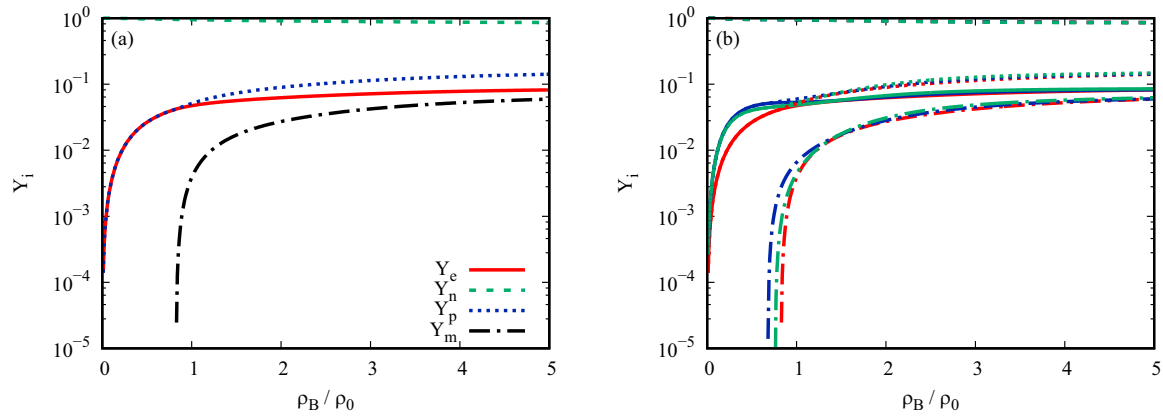

FIG. 4. Particle fractions of the constituents of the β-stable nuclear matter as a function of ρ_B/ρ_0 calculated in the E-RMF model for (a) the G3(M) parameters set and (b) the G3(M), TM1e, and FSU Garnet parameter sets, which are represented by different colors. Y_e, Y_n, Y_p, and Y_m represent respectively the electron, neutron, proton, and muon fractions.

The neutrino differential cross section is straightforwardly derived from the Lagrangian in Eq. (16) and it gives [21,22]

$$\frac{1}{V}\frac{d^3\sigma}{d^2\Omega' dE'_\nu} = -\frac{G_F}{32\pi^2}\frac{E'_\nu}{E_\nu}\mathrm{Im}[L_{\mu\nu}\Pi^{\mu\nu}], \tag{18}$$

with E_ν and E'_ν being the initial and final neutrino energies, respectively. The neutrino tensor $L_{\mu\nu}$ can be defined by

$$L_{\mu\nu} = 8[2k_\mu k_\nu + (k\cdot q)g_{\mu\nu} - (k_\mu q_\nu + q_\mu k_\nu) - i\epsilon_{\mu\nu\alpha\beta}k^\alpha q^\beta], \tag{19}$$

where the four-momentum transfer is defined as $q = (q_0, \mathbf{q})$ and k is the initial neutrino four-momentum. The polarization tensor $\Pi^{\mu\nu}$ for each target particle can be defined by [21,22]

$$\Pi^j_{\mu\nu} = -i\int \frac{d^4p}{(2\pi)^4}\mathrm{Tr}\big[G^j(p)\Gamma^j_\mu G^j(p+q)\Gamma^j_\nu\big], \tag{20}$$

where $p = (p_0, \boldsymbol{p})$ is the initial four-momentum of the target particles and $G^j(p)$ is the propagator of the target particle j, which is explicitly defined as

$$G^{n,p}(p) = (p^* + M^*)\left[\frac{1}{[p^{*2} - M^{*2} + i\epsilon]} + \frac{i\pi}{E^*}\delta(p_0^* - E^*)\Theta\big(p_F^{p,n} - |\boldsymbol{p}|\big)\right], \tag{21}$$

where the $E^* = \sqrt{\boldsymbol{p}^{*2} + M^{*2}} = E + \Sigma_0$ is the effective nucleon energy and $M^* = M + \Sigma_s$ is the nucleon effective mass, where Σ_s and Σ_0 are respectively the scalar and timelike self-energies. The nucleon effective momentum is defined as $\boldsymbol{p}^* = \boldsymbol{p} + (\frac{\boldsymbol{p}}{|\boldsymbol{p}|})\Sigma_v$, where $|\boldsymbol{p}|$ is the three-component momentum of the nucleon and Σ_v is the spacelike self-energy. Here $p_F^{p,n} = \sqrt{E_F^2 - M^{*2}}$ is the nucleon (proton and neutron) Fermi momentum.

The electron and muon propagators are taken to be the same as the free electron and muon propagators, respectively. The details of analytic derivations of the polarization tensors and the contractions of the leptonic and hadronic parts for the weak interaction as well as other quantities in Eq. (18) can be found in Refs. [6,24].

B. Neutrino mean free path

In this section, I present the NMFP of the neutrino scattering. The final expression for the inverse NMFP obtained by integrating the differential cross section of Eq. (18) over the energy transfer q_0 and the three-component momentum transfer $|\boldsymbol{q}|$ at a fixed baryon density can be obtained as [21,22]

$$\lambda(E_\nu)^{-1} = \int_{q_0}^{2E_\nu - q_0} d|\boldsymbol{q}| \int_0^{2E_\nu} dq_0 \frac{|\boldsymbol{q}|}{E'_\nu E_\nu}\frac{2\pi}{V}\frac{d^3\sigma}{d^2\Omega' dE'_\nu}, \tag{22}$$

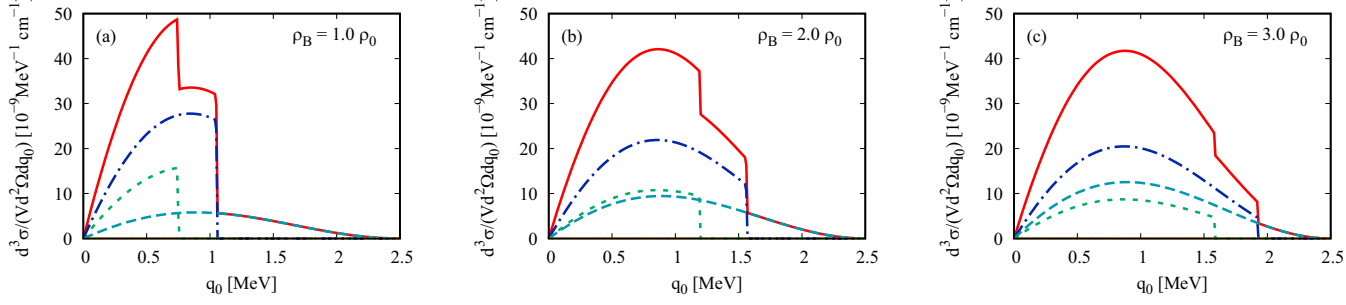

FIG. 5. DCRS of neutrinos as a function of q_0 for (a) $\rho_B = 1.0\ \rho_0$, (b) $\rho_B = 2.0\ \rho_0$, and (c) $\rho_B = 3.0\ \rho_0$ for the G3(M) parameter set at $|\boldsymbol{q}| = 2.5$ MeV and $E_\nu = 5$ MeV. The solid, dotted-dashed, dashed, long-dashed, and dotted lines are the differential cross sections of neutrinos for total (electrons + neutrons + protons + muons), neutrons, protons, electrons, and muon, respectively.

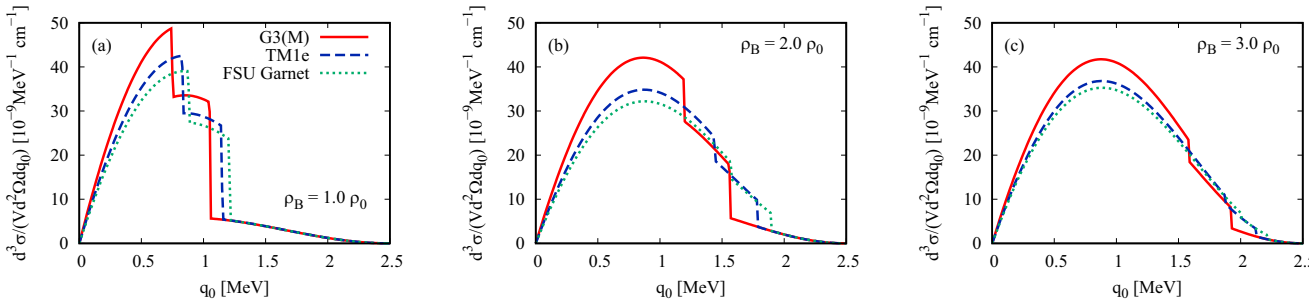

FIG. 6. Total DCRS of neutrinos as a function of q_0 for the same parameter sets as in Fig. 1 for (a) $\rho_B = 1.0\ \rho_0$, (b) $\rho_B = 2.0\ \rho_0$, and (c) $\rho_B = 3.0\ \rho_0$.

where the final and initial neutrino energies are related as $E'_\nu = E_\nu - q_0$. Further detailed explanations for the determination of the lower and upper limits of the integral can be found in Refs. [21,22].

IV. NUMERICAL RESULTS

Here the numerical results for the particle fractions of the constituents of β-stable matter, neutrino DCRS, and NMFP for the G3(M) parameter set are presented. The neutrino DCRS and NMFP are calculated with fixed values of the three-component transferred momentum $|\boldsymbol{q}| = 2.5$ MeV and the initial neutrino energy $E_\nu = 5$ MeV.

Results for the particle fractions of electrons, neutrons, protons, and muons as a function of ρ_B/ρ_0 for only the G3(M) parameter set are shown in Fig. 4(a). The particle fractions for all the parameter sets are shown in Fig. 4(b). The particle fractions of neutrons, protons, and electrons for the G3(M) parameter set are almost unchanged compared with the values obtained for the TM1e and FSU Garnet parameter sets. However, the appearance of muons for the G3(M) parameter set is rather longer than that obtained for the TM1e and FSU Garnet parameter sets, as shown in Fig. 4(b).

Next, in Fig. 5, the DCRS of neutrinos for the G3(M) parameter set as a function of the energy transferred momentum q_0 for different baryon densities (a) $\rho_B = 1.0\ \rho_0$, (b) $\rho_B = 2.0\ \rho_0$, and (c) $\rho_B = 3.0\ \rho_0$ are presented. The patterns of the DCRS of neutrinos for each constituent significantly change as the baryon density increases. Consequently, it leads to the change of the shape and magnitude of the total DCRS.

Compared with the total DCRS of neutrinos for the TM1e and FSU Garnet parameter sets, the G3(M) parameter set has a higher value of the cross section as shown in Figs. 6(a)–6(c). It shows that the DCRS of neutrinos are sensitive to the parameter set used. However, in general, the patterns of the DRCS of neutrinos for different parameters sets are rather the same.

The change of DCRS of neutrinos for each parameter set affects the NMFP as shown in Fig. 7. Figure 7(a) shows the NMFP for the G3(M) parameter set is lower than those obtained for the TM1e and FSU Garnet parameter sets. However, the NMFP for each parameters set decreases as the ρ_B/ρ_0 increases. Note that the higher NMFP is given by the FSU Garnet parameter set. An increasing DCRS or a decreasing NMFP is expected due to the nucleon effective mass M_N^* as shown in Fig. 7(b). The M_N^* value for the G3(M) parameter set is higher than the values obtained for the FSU Garnet and TM1e parameter sets, in particular, at higher densities.

V. SUMMARY

To summarize, I have studied the implications of the G3(M) parameter set that is constrained by PREX-2 data on the equation of state, particle fractions of constituents of the matter, differential cross section of the neutrino, and NMFP in the E-RMF model.

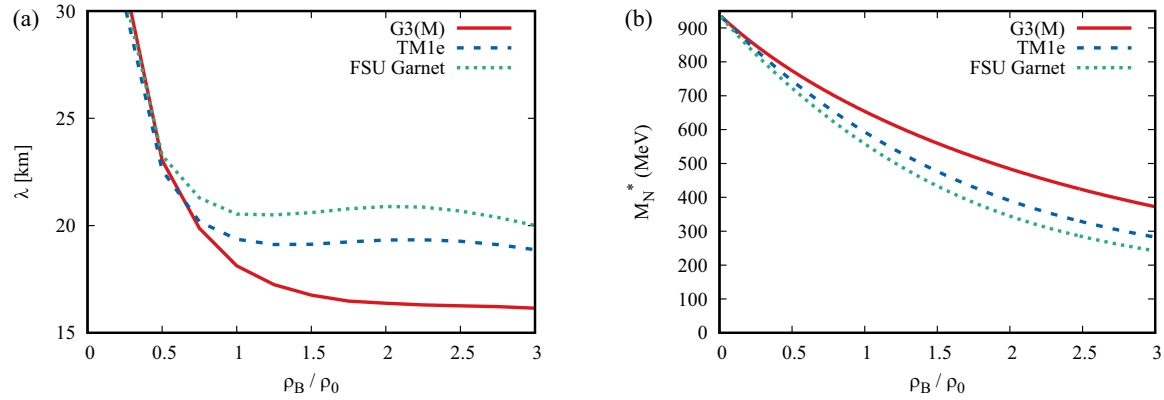

FIG. 7. NMFP (a) and nucleon effective mass M_N^* (b) as a function of ρ_B/ρ_0 for the G3(M), TM1e, and FSU Garnet parameter sets.

One finds that the binding energy per nucleon for the G3(M) parameter set is softer at low baryon density compared with those obtained for the TM1e and FSU Garnet parameter sets. In contrast, at higher baryon density, the binding energy for the G3(M) parameter set is stiffer than that obtained for the FSU Garnet parameter set and is the same as that obtained for the TM1e parameter set. The E_B/A value for the G3(M) parameter set fits well with the result of the chiral effective field theory calculation with N^3LO 3N forces [20], in particular, at higher densities.

Looking at the results for the pressure for pure neutron matter, one finds that the pressure for pure neutron matter for the G3(M) parameter set fits well with the asy-soft experimental data at intermediate baryon density. However, at higher baryon density, it has a good agreement with the asy-stiff data.

Looking at the results for the sound velocity, one finds that the sound velocity for the G3(M) parameter set is lower than those obtained for the TM1e and FSU Garnet parameter sets at intermediate ρ_B/ρ_0, but it is higher at higher ρ_B/ρ_0.

One finds the differential cross sections of neutrinos for different densities with the G3(M) parameter set have higher values compared with those obtained for the TM1e and FSU Garnet parameter sets, and a higher cross section value decreases the neutrino mean free path.

ACKNOWLEDGMENTS

P.T.P.H. thanks A. Sulaksono for valuable conversation and discussion and Seung-Il Nam for useful conversation. This work was supported by the National Research Foundation of Korea (NRF) funded by the Korea government (MSIT), Grants No. 2018R1A5A1025563 and No. 2019R1A2C1005697.

[1] D. G. Yakovlev, A. D. Kaminker, O. Y. Gnedin, and P. Haensel, Neutrino emission from neutron stars, Phys. Rep. **354**, 1 (2001).
[2] A. Burrows and J. M. Lattimer, Neutrinos from SN 1987A, Astrophys. J. Lett. **318**, L63 (1987).
[3] P. T. P. Hutauruk, A. Sulaksono, and K. Tsushima, Effect of neutrino magnetic moment and charge radius on the neutrino mean free path in dense matter with medium modifications of the nucleon form factors, arXiv:2009.08781.
[4] P. T. P. Hutauruk, Y. Oh, and K. Tsushima, Effects of medium modifications of nucleon form factors on neutrino scattering in dense matter, JPS Conf. Proc. **26**, 024031 (2019).
[5] P. T. P. Hutauruk, Y. Oh, and K. Tsushima, Impact of medium modifications of the nucleon weak and electromagnetic form factors on the neutrino mean free path in dense matter, Phys. Rev. D **98**, 013009 (2018).
[6] S. Reddy, M. Prakash, and J. M. Lattimer, Neutrino interactions in hot and dense matter, Phys. Rev. D **58**, 013009 (1998).
[7] R. Niembro, P. Bernardos, M. Lopez-Quelle, and S. Marcos, Neutrino cross-section and mean free path in neutron stars in the framework of the Dirac-Hartree-Fock approximation, Phys. Rev. C **64**, 055802 (2001).
[8] D. Adhikari *et al.* (PREX Collaboration), Accurate Determination of the Neutron Skin Thickness of ^{208}Pb through Parity-Violation in Electron Scattering, Phys. Rev. Lett. **126**, 172502 (2021).
[9] S. Abrahamyan, Z. Ahmed, H. Albataineh, K. Aniol, D. S. Armstrong, W. Armstrong, T. Averett, B. Babineau, A. Barbieri, V. Bellini *et al.* (PREX Collaboration), Measurement of the Neutron Radius of ^{208}Pb through Parity-Violation in Electron Scattering, Phys. Rev. Lett. **108**, 112502 (2012).
[10] J. A. Pattnaik, R. N. Panda, M. Bhuyan, and S. K. Patra, Constraining the relativistic mean-field models from PREX-2 data: Effective forces revisited, arXiv:2105.14479.
[11] B. T. Reed, F. J. Fattoyev, C. J. Horowitz, and J. Piekarewicz, Implications of PREX-2 on the Equation of State of Neutron-Rich Matter, Phys. Rev. Lett. **126**, 172503 (2021).
[12] J. Piekarewicz, Implications of PREX-2 on the electric dipole polarizability of neutron-rich nuclei, Phys. Rev. C **104**, 024329 (2021).
[13] B. Kumar, S. K. Singh, B. K. Agrawal, and S. K. Patra, New parameterization of the effective field theory motivated relativistic mean field model, Nucl. Phys. A **966**, 197 (2017).
[14] B. K. Agrawal, A. Sulaksono, and P. G. Reinhard, Optimization of relativistic mean field model for finite nuclei to neutron star matter, Nucl. Phys. A **882**, 1 (2012).
[15] R. J. Furnstahl, B. D. Serot, and H. B. Tang, Analysis of chiral mean field models for nuclei, Nucl. Phys. A **598**, 539 (1996).
[16] S. S. Bao, J. N. Hu, Z. W. Zhang, and H. Shen, Effects of the symmetry energy on properties of neutron star crusts near the neutron drip density, Phys. Rev. C **90**, 045802 (2014).
[17] W. C. Chen and J. Piekarewicz, Searching for isovector signatures in the neutron-rich oxygen and calcium isotopes, Phys. Lett. B **748**, 284 (2015).
[18] P. Danielewicz, R. Lacey, and W. G. Lynch, Determination of the equation of state of dense matter, Science **298**, 1592 (2002).
[19] R. J. Furnstahl, B. D. Serot, and H. B. Tang, A chiral effective Lagrangian for nuclei, Nucl. Phys. A **615**, 441 (1997); A chiral effective Lagrangian for nuclei, *ibid.* **640**, 505E (1998).
[20] I. Tews, T. Krüger, K. Hebeler, and A. Schwenk, Neutron Matter at Next-to-Next-to-Next-to-Leading Order in Chiral Effective Field Theory, Phys. Rev. Lett. **110**, 032504 (2013).
[21] A. Sulaksono, P. T. P. Hutauruk, and T. Mart, Isovector-channel role of relativistic mean field models in the neutrino mean free path, Phys. Rev. C **72**, 065801 (2005).
[22] C. J. Horowitz and K. Wehrberger, Neutrino neutral current interactions in nuclear matter, Nucl. Phys. A **531**, 665 (1991).
[23] P. T. P. Hutauruk, C. K. Williams, A. Sulaksono, and T. Mart, Neutron fraction and neutrino mean free path predictions in relativistic mean field models, Phys. Rev. C **70**, 068801 (2004).
[24] P. T. Hutauruk, Neutrino mean free path in neutron star, arXiv:1007.4007.